Electronic Supplementary Material (ESI) for RSC Advances.
This journal is © The Royal Society of Chemistry 2020

Supporting Information For

A pH-stable Ag(I) multifunctional luminescent sensor for the efficient detection of organic solvents, organochlorine pesticides and heavy metal ions

Jianxin Ma,[a] Yue Wang,[a] Guocheng Liu,[a] Na Xu*[a] and Xiuli Wang*[a]

[a] College of Chemistry and Materials Engineering, Bohai University, Liaoning Professional Technology Innovation Center of Liaoning Province for Conversion Materials of Solar Cell, Jinzhou 121013, P. R. China

S1. X-ray Crystallography

The single-crystal diffraction data for LCP **1** was collected by using a Bruker SMART APEXII CCD diffractometer at 293 K with Mo Kα radiation (λ = 0.71073 Å). The initial structure was solved by direct methods using the SHEL-XS program of the SHELX-TL package.[1] All crystal data and detailed structural refinement results are summarized in Table S1, and selected bond lengths (Å) and angles (°) are listed in Table S2. The crystallographic data for CP_**1** has been obtained as 2035795 from the Cambridge Crystallographic Data Center free of charge *via* https://www.ccdc.cam.ac.uk.

Table S1. Crystallographic data for LCP **1**.

LCP	**1**
Empirical formula	$C_{32}H_{29}N_4AgO_{12}$
Formula weight	769.46
Crystal system	Triclinic
Space group	*P-1*
a (Å)	8.492(6)
b (Å)	13.445(6)
c (Å)	13.518(6)
α (°)	83.690(9)
β(°)	86.778(9)
γ (°)	85.131(6)
V (Å ^{3})	1526.8(14)
Z	2
D_{calc} (g/cm^3)	1.674
μ/mm^{-1}	0.735
F(000)	784
R_{int}	0.0529

R_1[a] [I>2σ(I)]	0.0842
wR_2[b](all data)	0.2803
GOF	0.981
$\Delta\rho_{max}$(e·Å^{-3})	1.841 and -0.851
R1,[a] wR_2[b] [I > 2σ(I)]	0.0842, 0.2376
R1,[a] wR_2[b] (all data)	0.1548, 0.2803

[a]$R_1 = \sum||F_o| - |F_c||/\sum|F_o|$. [b]$wR_2 = [\sum w(F_o^2 - F_c^2)^2/\sum w(F_o^2)^2]^{1/2}$.

Table S2. Selected bond lengths (Å) and bond angles (°) for LCP **1**.

LCP **1**			
Ag(1)–N(1)	2.123(8)	Ag(1)–O(1)	2.721(7)
Ag(1)–N(2) #1	2.155(8)	N(2)#1–Ag(1)–O(1)	90.6(3)
N(1)–Ag(1)–N(2)#1	168.1(3)	N(1)–Ag(1)–O(1)	96.7(3)
Symmetry codes: #1 x+1, y, z–1			

Table S3. Hydrogen-bonding geometry (Å, °) for LCP **1**.

D–H···A	D–H	H···A	D···A	D –H···A
O(8)-H(8)···O(3)	0.82	1.80	2.492(12)	142
O(5)-H(5)···O(2)	0.82	2.31	3.023(11)	145

Table S4. Comparison of fluorescent property of LCP **1** for sensing Hacac.

Fluorescent sensing materials	K_{sv} (M^{-1})	Detection Limit (M)	Medium	Ref.
LCP **1**	1.542×10^4	1.517×10^{-5}	EtOH	This work
$[Zn_4(3\text{-dpyb})_2(odpa)_2(H_2O)_3]\cdot4H_2O$	2.1721×10^5	5.244×10^{-6}	EtOH	2
$[Zn_4(3\text{-dpyb})_2(odpa)_2(H_2O)_3]\cdot4H_2O$	2.872×10^4	3.956×10^{-5}	H_2O	2
Co-CP	1.04×10^4	2.3×10^{-3}	EtOH	3
Co-CP	2.86×10^3	6.9×10^{-3}	H_2O	3
$\{[Zn(XL)_2](ClO_4)_2\cdot6\,H_2O\}_n$	2.3×10^3	5.0×10^{-6}	DMF	4
$\{[Zn_3(BBIB)_2(NDC)_3]\cdot2DMF\cdot2H_2O\}_n$		1.00×10^{-7}	DMF	5

Table S5. Comparison of fluorescent property of LCP **1** for sensing NB.

Fluorescent sensing materials	K_{sv} (M^{-1})	Detection Limit (M)	Medium	Ref.
LCP **1**	1.683×10^4	1.391×10^{-5}	EtOH	This work
$[Zn_4(3\text{-dpyb})_2(odpa)_2(H_2O)_3]\cdot4H_2O$	1.037×10^5	1.098×10^{-5}	EtOH	2
$\{[Zn(dip)(hdin)]\cdot2.5H_2O\}_n$	1.0×10^6	-	EtOH	6
$\{[Zn(dip)(pedin)]\cdot2.5H_2O\}_n$	2.0×10^6	-	EtOH	6
$[Cd(TPA)(DIB)]_n$	1.7×10^4	2.7×10^{-7}	DMA	7
$\{[Zn(H_4L)(bpy)0.5(H_2O)_2]\cdot H_2O\}_n$	8.8×10^3	-	DMA	8
$\{[Zn_6(L)_2(H_2O)_7]\cdot(DMF)_2\}_n$	7.88×10^3	-	DMA	8

Table S6. Comparison of fluorescent property of LCP **1** for sensing 2,6-DCN.

Fluorescent sensing materials	K_{sv} (M^{-1})	Detection Limit (M)	Medium	Ref.

LCP **1**	2.028×10^{5}	1.154×10^{-6}	EtOH	This work
$[Zn(L)(1,4\text{-BDC})]\cdot H_2O$	2.78×10^{4}	1.19×10^{-4}	DMF	9
$[Zn(L)(1,3\text{-BDC})]\cdot H_2O$	4.88×10^{4}	8.05×10^{-5}	DMF	9
$[Zn(L)(1,2\text{-BDC})]$	4.1×10^{4}	1.154×10^{-6}	DMF	9
$[Cd(L)_{0.5}(1,2\text{-BDC})(H_2O)]$	3.34×10^{4}	8.1×10^{-5}	DMF	9
$[Ag(CIP^{-})]$	5.2×10^{4}	1.05×10^{-4}	DMF	10
$[Mg_2(APDA)_2(H_2O)_3]\cdot 5DMA\cdot 5H_2O$	7.5×10^{4}	1.50×10^{-4}	DMF	11
$[Zn_2(L)_2(TPA)]2H_2O$	2.36×10^{4}	3.9×10^{-6}	MeOH	12

Table S7. Comparison of fluorescent property of LCP **1** for sensing Fe^{2+}.

Fluorescent sensing materials	K_{sv} (M^{-1})	Detection Limit (M)	Medium	Ref.
LCP **1**	6.107×10^{4}	3.831×10^{-6}	H_2O	This work
(E)-2-((pyren-1-ylmethylene)amino)benzenethiol	3.04×10^{9}	0.3 ppm	CH_3CN	13
8-hydroxyquinoline-based chemosensor	-	5.6×10^{-7}	EtOH/THF	14
HBTC	-	2.03×10^{-6}	THF	15

Table S8. Comparison of fluorescent property of LCP **1** for sensing Hg^{2+}.

Fluorescent sensing materials	K_{sv} (M^{-1})	Detection Limit (M)	Medium	Ref.
LCP **1**	1.005×10^{5}	2.328×10^{-6}	H_2O	This work
$\{[Zn(dip)(edin)]\cdot 3H_2O\}_n$	1.0×10^{6}	3.15×10^{-6}	H_2O	6
NO_2/Dan_4	-	1.0×10^{-4}	MeCN	16
$[Zn(OBA)(DPT)_{0.5}]\cdot$DMF (TMU-34(-2H)	-	6.9×10^{-6}	acetonitrile	17
Thiocoumarin derivatives	-	1.7×10^{-6}	H_2O/MeCN	18
2,3-diphenylpyrido[2,3-b]pyrazine	-	1.06×10^{-6}	H_2O	19
2-SBA-15		3.36×10^{-7}	H_2O	20

Table S9. Comparison of fluorescent property of LCP **1** for sensing Fe^{3+}.

Fluorescent sensing materials	K_{sv} (M^{-1})	Detection Limit (M)	Medium	Ref.
LCP **1**	1.186×10^{5}	1.973×10^{-6}	H_2O	this work
$[Zn_4(3\text{-dpyb})_2(odpa)_2(H_2O)_3]\cdot 4H_2O$	9.129×10^{5}	1.247×10^{-7}	H_2O	2
$[Zn(L)(1,4\text{-BDC})]\cdot H_2O$	5.8×10^{4}	5.7×10^{-5}	H_2O	8
$[Zn(L)(1,3\text{-BDC})]\cdot H_2O$	3.74×10^{4}	8.82×10^{-5}	H_2O	8
$[Zn(L)(1,2\text{-BDC})]$	4.36×10^{4}	7.57×10^{-5}	H_2O	8
$\{[Eu_2(ppda)_2(npdc)(H_2O)]\cdot H_2O\}_n$	1.64×10^{5}	1.66×10^{-5}	H_2O	21
$\{[Zn_2(L)_2(TPA)]\cdot 2H_2O\}_n$	6.4×10^{3}	3.84×10^{-6}	EtOH	22
$\{Cd(MDIP)(H_2O)_2\}_n$	4.13×10^{4}	8.0×10^{-9}	H_2O	23
EuL_3	4.1×10^{3}	-	H_2O	24
BUT-14	2.17×10^{3}	-	H_2O	25

Table S10. Determination of Fe^{2+}, Hg^{2+} and Fe^{3+} in river water samples.

Metal ions	Spiked (μM)	Found (μM)	Recovery (%)
Fe^{2+}	5	5.01	100.20
	10	9.62	96.20
	15	14.96	99.73
Hg^{2+}	5	5.11	102.20
	10	10.12	101.2
	15	14.96	99.73
Fe^{3+}	5	5.03	100.06
	10	10.15	101.50
	15	15.65	104.33

Scheme S1. Synthesis method of LCP **1**.

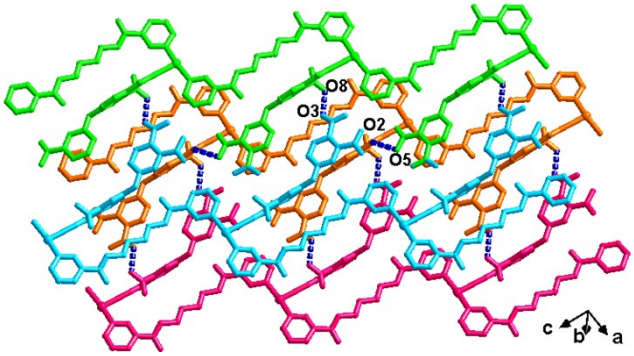

Fig. S1. View of 3D supramolecular architecture of LCP **1**.

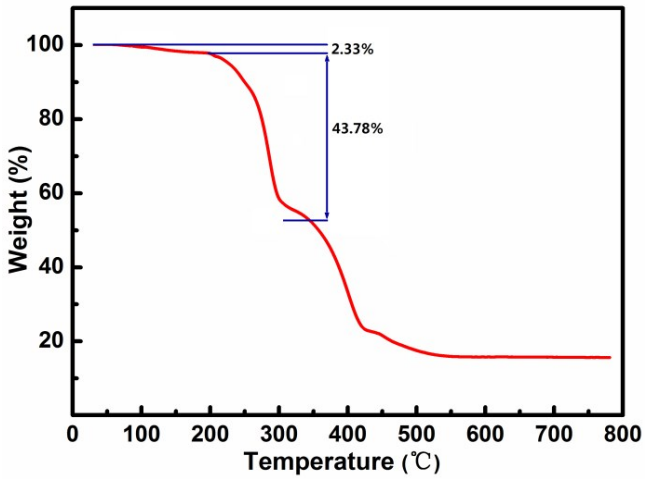

Fig. S2. The TGA curve of LCP **1**.

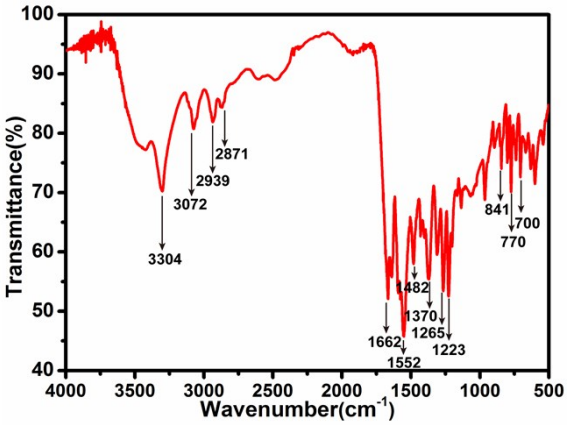

Fig. S3. The IR spectra of LCP **1**.

Table S11. Various IR bands for functional groups of LCP **1**.

Wavenumber (cm^{-1})	Functional group
3304	–OH
3072, 2939, and 2871	$–CH_2–$
1662	–COOH
1552 1482, and 1370	$–COO^-$
1265 and 1223	–C–N–
841, 770, and 700	N-heterocyclic rings

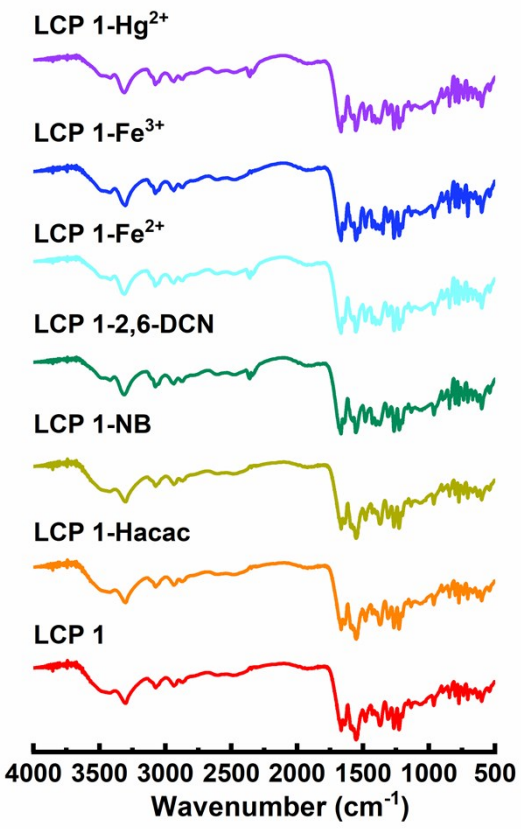

Fig. S4. The IR spectra of LCP **1** before and after being soaked in different analytes.

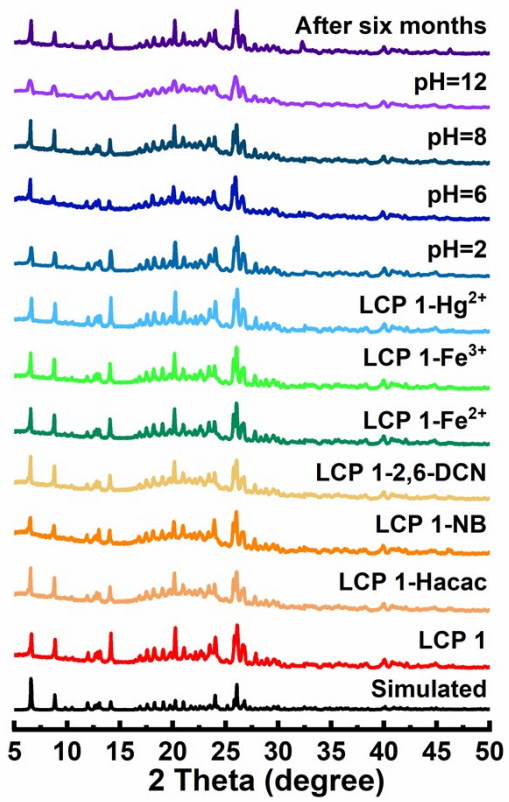

Fig. S5. The PXRD pattern of LCP **1** (black: simulated from the X-ray single-crystal data, red: synthesized) before and after exposure to different analytes, after being soaked in water, acidic, and basic solutions for 24 h using a wide pH range of 2.0 ~ 12.0, and placed in air for about 6 months.

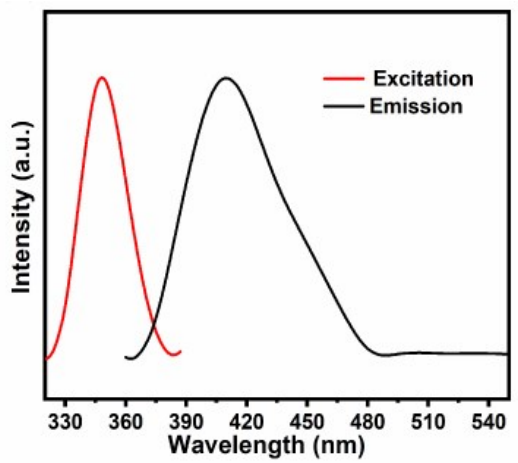

Fig. S6. The solid excitation and emission spectra of LCP **1**.

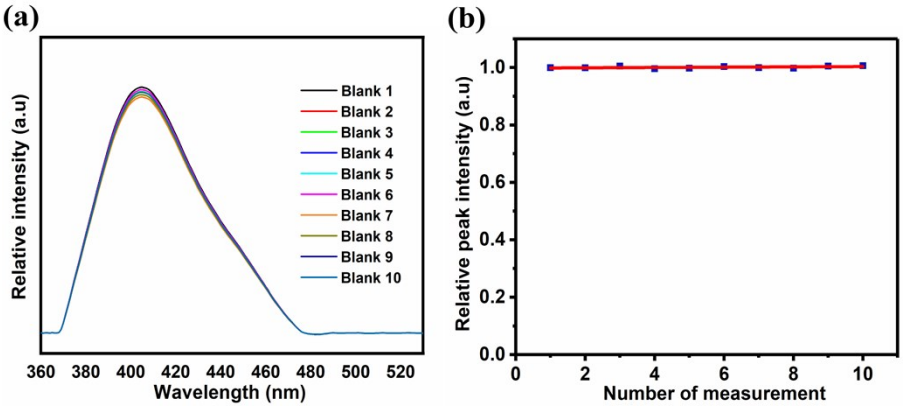

Fig. S7. (a) The photoluminescence spectra from ten cycles blank measurements for solid state of LCP **1**; (b) Calibration curve with blank measurements after ten cycles (insert: the standard deviation formula, where x, $\bar{x}$ and n represent the luminescence intensity values of LCP **1** after normalization, the average of the maximum luminescence intensity values of LCP **1** after ten cycles and the cycles of blank measurements, respectively). Calculated standard deviation, δ = 0.07856.

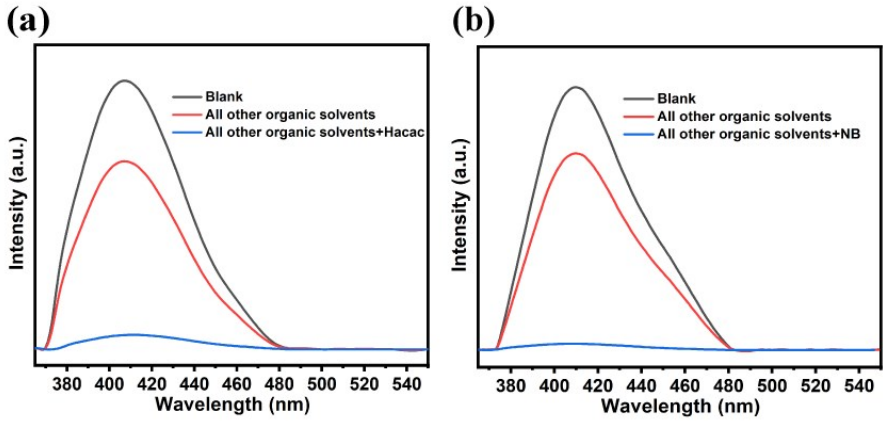

Fig. S8. The effect of adding other organic solvents on the luminescence intensity of (a) Hacac and (b) NB.

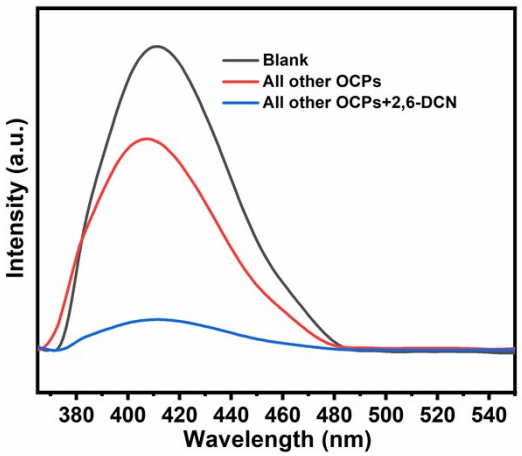

Fig. S9. The effect of adding other OCPs on the luminescence intensity of 2,6-DCN.

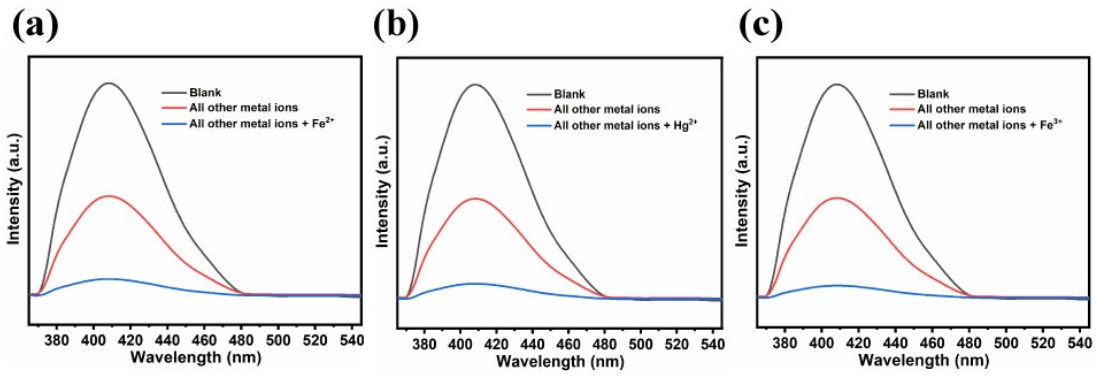

Fig. S10. The effect of adding other metal ions on the luminescence intensity of (a) Fe^{2+}, (b) Hg^{2+} and (c) Fe^{3+}.

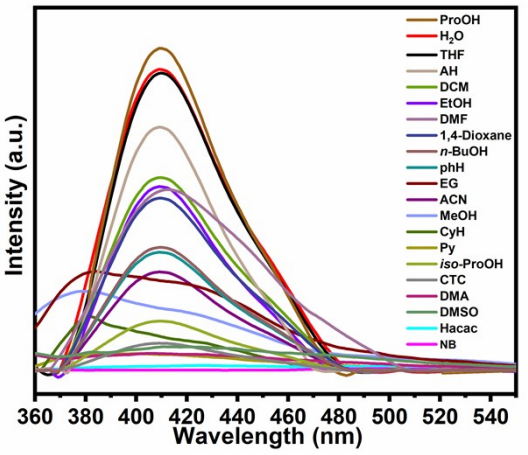

Fig. S11. Luminescence intensity of LCP **1** in different organic solvents.

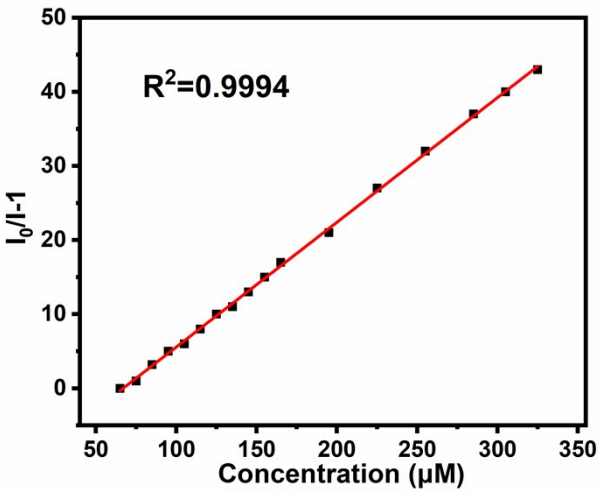

Fig. S12. The Stern-Volmer plot of I_0/I-1 *vs.* the concentration of 2,6-DCN.

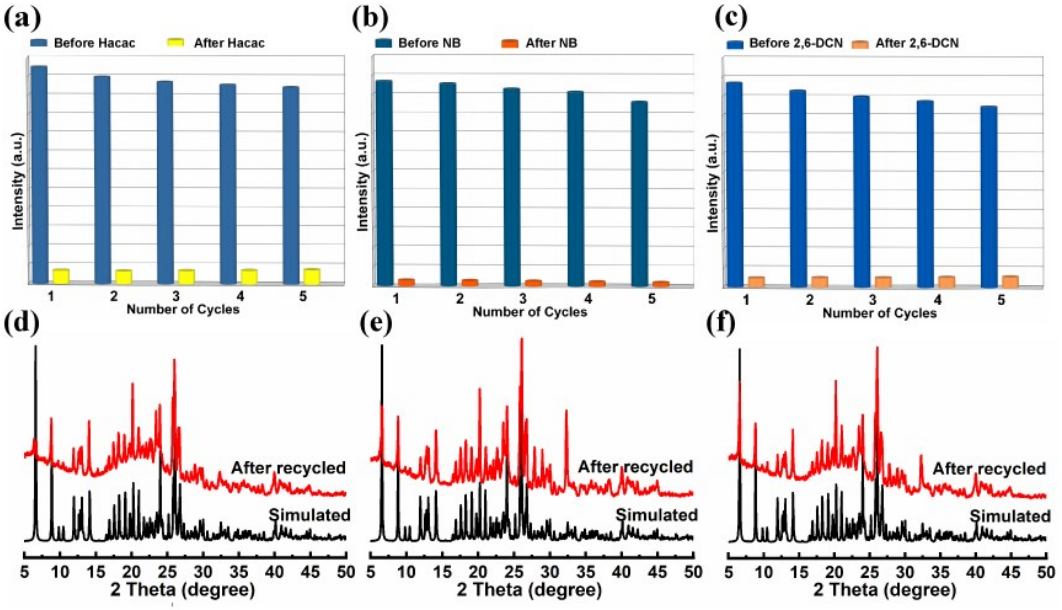

Fig. S13. The cyclic response of the luminescence intensities of LCP **1** for detecting Hacac (a), NB (b) and 2,6-DCN (c); The PXRD patterns of LCP **1** treated by the Hacac (d), NB (e) and 2,6-DCN (f).

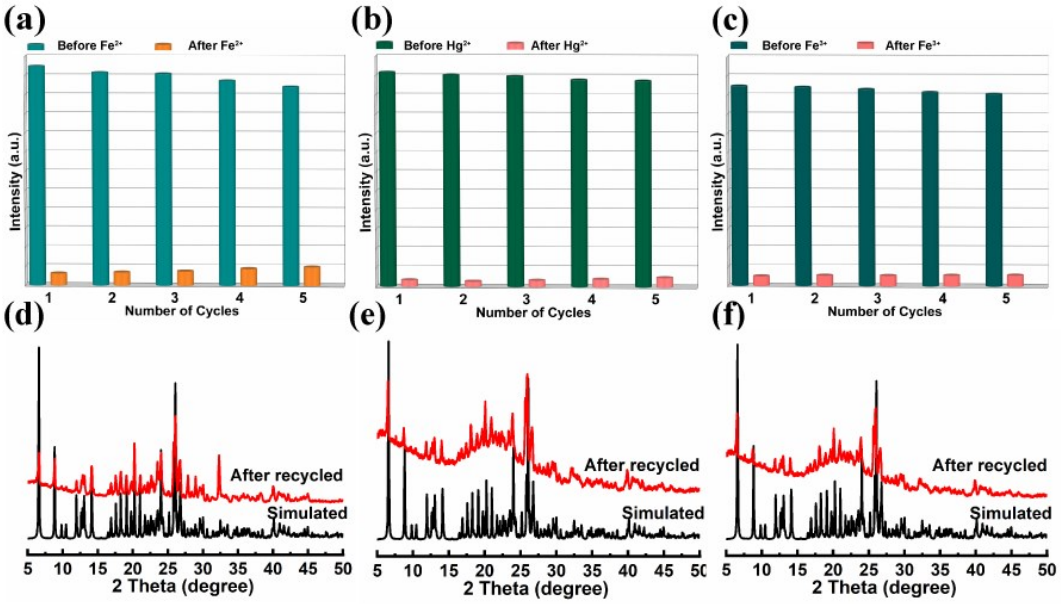

Fig. S14. The cyclic response of the luminescence intensities of LCP **1** for detecting of Fe^{2+} (a), Hg^{2+} (b) and Fe^{3+} (c); The PXRD patterns of LCP **1** treated by the of Fe^{2+} (d), Hg^{2+} (e) and Fe^{3+} (f).

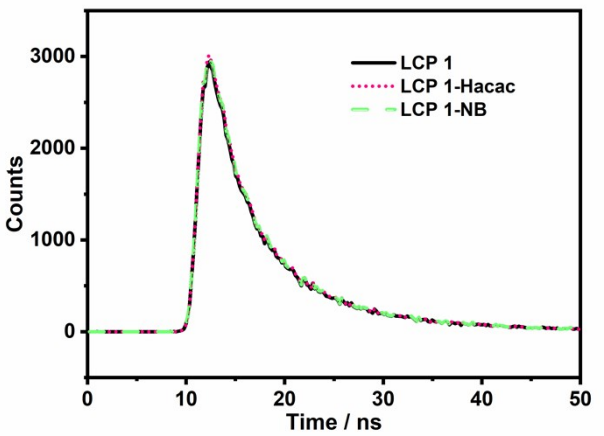

Fig. S15. Lifetime decay curves of LCP **1** before and after the addition of two analyses.

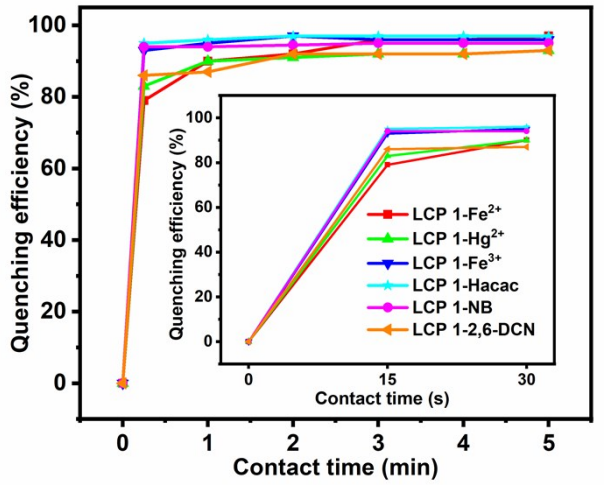

Fig. S16. Time-dependent fluorescence quenching percentage by six analyses from 0–5 minutes. (Inset: from 0–30 seconds).

References

1. G. M. Sheldrick, *Acta Cryst*, 2008, **64**, 112-122.
2. J. X. Ma, N. Xu, Y. Liu, Y. Wang, H. Li, G.C. Liu, X.L. Wang, J. R. Li, Inorg Chem, 2020, 59, 15495-15503.
3. Q. Q. Xiao, G. Y. Dong, Y. H. Li, *Inorg. Chem*, 2019, **58**, 15696-15699.
4. X. M. Kang, X. Y. Fan, P. Y. Hao, *Inorg Chem Front*., 2019, **6**, 271-277.
5. S. L. Yao, S. J. Liu, X. M. Tian, T. F. Zheng, C. Cao, C. Y. Niu, Y. Q. Chen and H. R. Wen, *Inorg. Chem*., 2019, **58**, 3578-3581.
6. B. L. Martinez, A. D. Shrode, R. J. Staples, R. L. LaDuca, Polyhedron, 2018, **151**, 369-380.
7. X. Wang, Y. Han, X. X. Han, *New J Chem*, 2018, **42**, 19844-19852.
8. X. D. Duan, F. Y. Ge, H. G. Zheng, *Inorg. Chem. Commun.*, 2019, **107**, 107479.
9. G. C. Liu, S. W. Han, Y. Gao, N, Xu, X. L. Wang, B. K. Chen. 10.1039/d0ce01351j
10. D. D. Feng, Y. D. Zhao, X. Q. Wang, D. D. Fang, J. Tang, L. M. Fan and J. Yang, *Dalton Trans*., 2019, **48**, 10892-10900.

11. N. Xu, Q. H. Zhang, B. S. Hou, Q. Cheng and G. A. Zhang, *Inorg. Chem*., 2018, **57**, 13330-13340.
12. H. He, S. H. Chen, D. Y. Zhang, R. Hao, C. Zhang, E. C. Yang and X. J. Zhao, *Dalton Trans.,* 2017, **46**, 13502-13509.
13. S. Pandey, A. Azam, S. Pandey and H. M. Chawla, *Org. Biomol. Chem.*, 2009, **7**, 269-279.
14. S. A. A. Razavi, M. Y. Masoomi, A. Morsali, *Inorg. Chem.,* 2017, **56**, 9646-9652.
15. M. G. Choi, Y. H. Kim, J. E. Namgoong and S. K. Chang, *Chem. Commun.*, 2009, **24**, 3560-3562.
16. K. Xu, Y. Li, Y. Si, Y. He, J. Ma, J. He, H. Hou and K. A. Li, *J. Lumin.*, 2018, **204**, 182-188.
17. R. M. Tivier, I. Leray, B. Lebeau, and B. Valeurab, *J. Mater. Chem*., 2005, **15**, 2965-2973.
18. C. F. Wan, Y. J. Chang, C. Y. Chien, Y. W. Sie, C. H. Hu, A. T. Wu, *J. Lumin.*, 2016, **178**, 115-120.
19. N. Lashgari, A. Badiei, G. Mohammadi Ziarani, *J. Fluoresc.*, 2016, **26**, 1885-1894.
20. S. Cetindere, S.O. Tümay, A, et al., *J. Fluoresc*., 2016, **26**, 1173-1181.
21. Z. Zhan, X. Liang, X. Zhang, Y. Jia, M. Hu, *Dalton Trans*., 2019, **48**, 1786-1794.
22. X. Y. Guo, Z. P. Dong, F. Zhao, Z. L. Liu, Y. Q. Wang, *New J. Chem*., 2019, **43**, 2353-2361.
23. Y. Li, Z. Chang, F. Huang, P. Wu, H. Chu, J. Wang, *Dalton Trans*., 2018, **47**, 9267-9273.
24. M. Zheng, H. Tan, Z. Xie, L. Zhang, X. Jing, Z. Sun, *ACS Appl. Mater. Interfaces*., 2013, **5**, 1078-1083.
25. B. Wang, Q. Yang, C. Guo, Y. Sun, L. H. Xie, J. R. Li, *ACS Appl. Mater. Interfaces*., 2017, **9**, 10286-10295.